ELSEVIER

Microchemical Journal 71 (2002) 221–230

MICROCHEMICAL JOURNAL

www.elsevier.com/locate/microc

Bulk-sensitive XAS characterization of light elements: from X-ray Raman scattering to X-ray Raman spectroscopy

Uwe Bergmann[a,b,*], Pieter Glatzel[b], Stephen P. Cramer[a,b]

[a]*MS 6-2100, 1 Cyclotron Rd., Lawrence Berkeley National Laboratory, Berkeley, CA 94720, USA*
[b]*Department of Applied Science, University of California, Davis, CA 95616, USA*

Accepted 10 December 2001

Abstract

X-Ray absorption spectroscopy (XAS) is a powerful tool for element-specific characterization of local structure and chemistry. Although application of XAS in the hard X-ray region is now routine, the soft X-ray region (containing light-element K-edges) presents a number of experimental problems. Most of the difficulties, including surface sensitivity, restricted sample environments, and radiation damage, stem from the submicron path lengths of soft X-rays and/or electrons. X-Ray Raman scattering (XRS) provides a means for obtaining the information content of soft X-ray spectra while maintaining the experimental benefits of hard X-ray techniques. In the XRS process, an incident photon is inelastically scattered and part of its energy is transferred to excite an inner shell electron into an unoccupied state. Under the dipole approximation, the resulting features are identical to the corresponding XAS spectrum. In the past, the extremely low cross-section of XRS has made this technique impractical, but intense new X-ray facilities and improvements in X-ray optics have helped to put XRS on the brink of becoming a routine spectroscopic tool. At present, high-quality X-ray Raman spectra can be obtained in minutes to hours. X-Ray Raman spectroscopy thus represents a hard X-ray alternative to conventional XAS techniques in the study of systems with light elements, including C, N and O. In this review we describe the technique, present examples of recent work, and discuss the prospects for the future.

Keywords: Bulk-sensitive XAS characterization; Light elements; X-Ray Raman scattering; X-Ray Raman spectroscopy; Inelastic X-ray scattering

1. Introduction

Intense and tunable synchrotron radiation (SR) sources have helped X-ray absorption spectroscopy (XAS) flourish over the past several decades. It is now a widely applied probe of local molecular and electronic structure. XAS is usually divided into X-ray absorption near edge structure (XANES) and extended X-ray absorption fine structure (EXAFS) regions (although the term XAFS is now employed to describe both phenomena). In this paper, we emphasize the use of X-ray Raman scattering (XRS) to obtain

*Corresponding author. Tel.: +1-510-486-6094; fax: +1-510-486-5664.
E-mail address: ubergmann@lbl.gov (U. Bergmann).

0026-265X/02/$ - see front matter
PII: S0026-265X(02)00014-0

bulk-sensitive XANES on low Z (<10) materials. However, the underlying mechanisms also hold for the EXAFS regime and for higher Z materials.

Light-atom XANES spectra are commonly measured in transmission, Auger yield, electron yield, sample photocurrent or fluorescence excitation modes [1]. Each method has its advantages and limitations. Due to the submicron path lengths of soft X-rays, transmission measurements require very thin samples that are sometimes difficult to prepare. For example, the absorption length of carbonaceous material above its K edge energy can be less than 0.1 μm. The samples should also be transversely homogeneous, and limited sensitivity restricts experiments to relatively concentrated systems. To simplify sample preparation, the various electron detection methods are often employed. However, these methods have probe depths of less than 50 Å and are thus surface sensitive [2]. In fact they might provide information about an oxide coating or sorbed atoms rather than about the bulk sample. Fluorescence yield probes deeper into the sample, but it can suffer from artifacts due to 'saturation effects' in concentrated systems [3] or from variations in fluorescence yield across the absorption edge [4].

These considerations show that there is a large class of systems and experimental conditions where the bulk properties are difficult to probe by conventional XANES methods. This class includes heterogeneous concentrated compounds, reactive materials, liquids, and systems under extreme pressure or temperature. Higher energy X-ray probes have several advantages for such samples, including 'bulk' ($\sim$mm) sensitivity and less stringent requirements on the sample environment. Equipment such as flow tubes, furnaces, in situ chambers and high-pressure cells have all been employed in the 5–10 keV range. X-Ray Raman scattering is a technique that can retain all of the experimental advantages of hard X-ray measurements, while still revealing the special information that is contained in the soft X-ray absorption spectra.

2. A brief history

> …I would like to call attention to observations of B. B. Ray [5–7], which have not, however, been confirmed by others [8,9]. They concern the passage of Röntgen rays through very thin layers, e.g., of carbon, which resulted in the formation of a 'very weak, broad, diffuse' line on the long wave-length side of the primary line, which 'appeared to have a more or less definite edge on its short wave side'.
>
> (Sommerfeld to Compton, 1936 [10]).

Immediately after the observation of Raman scattering in the visible region, researchers began looking for the X-ray version of this effect, which was first mentioned by Smekal in 1923 [11]. Davis and Mitchell [12] reported the observation of shifted lines when analyzing scattered Mo $K\alpha_1$ radiation from graphite. One of the observed lines appeared 279 eV below the elastic Rayleigh scattering line, seemingly corresponding to inelastic scattering involving the promotion of a C 1s electron to an empty state. However, two subsequent studies [13,14] could not reproduce this result, and the explanation by Ehrenberg [13], assigning the observed signal to Lβ fluorescence from a small uranium contamination, was probably correct. The putative 'Raman' line had been much too strong. However, without a tunable source, the test to discriminate fluorescence from inelastic scattering was not trivial.

The hunt continued. In 1950, Das Gupta noted in a letter to Nature that 'The new type of scattering would probably be better detected when the involved beam is more or less monochromatic' [15]. Starting with the work on polystyrene [15a], several reports confirmed the observation of the effect [16–18]. It was also Das Gupta who, quite appropriately in our opinion, used the name Smekal–Raman modified X-ray scattering [15a]. Still, in the mid-1960s, there was at least one study reporting a negative result [19]. Finally, the theoretical work by Mizuno and Ohmura [20] and experiments by Suzuki [21] clearly established the close connection between XRS and XAS. In fact, it is argued in the later literature [22] that Suzuki's experiments on elements from Be to C were the first to show unambiguous X-ray Raman spectra.

The first demonstrations of XRS for spectroscopic applications appeared when SR became more widely available. Using 8–9 keV X-rays, Tohji and Udagawa were able to obtain an EXAFS-like XRS spectrum from graphite with 6 eV resolution [22,23]. Schülke et al. studied interband

transitions and core excitations in oriented graphite with 0.8 eV resolution at ~8 keV. More recently, several groups have applied XRS to look at the B and N K-edges of hexagonal boron nitride [24], the K-edge of Li metal [25], the C K-edge of asphaltenes [26,27], and the O K-edge [28,29], and valence transitions [30,31] of water. The potential of XRS has clearly been recognized, and third-generation SR facilities such as ESRF, APS and SPring-8 have programs to build dedicated inelastic scattering beamlines. Below, we will show (with a chemical emphasis) what is possible today.

3. XRS theory

A comparison of the XRS process with other scattering events is shown in Fig. 1. In general, an incident photon with energy E_0 is scattered with energy loss ΔE, yielding a photon with final energy E_f. Varying $\Delta E = E_0 - E_f$ by changing the incident energy at a fixed analyzer energy set to E_f results in a spectrum with three main components (Fig. 1). The strongest feature is the elastic Rayleigh scattering peak at $\Delta E = 0$. Next is the broad Compton spectrum from inelastic scattering on valence electrons. Finally, riding on the Compton background is the XRS spectrum containing the X-ray Raman events, where energy transfer, ΔE, results in the excitation of a core electron. The Raman cross-section is clearly much smaller than those for Rayleigh or Compton scattering.

The graphite spectrum shown in Fig. 1 was taken at beamline X-25 at the National Synchrotron Light Source, with a total resolution of 2.5 eV FWHM (see quasi-elastic peak). The transition probability for XRS, w, is described by [22]:

$$w = \{(4\pi^3 e^4 h)/(m^2 v_i v_j)\}(1+\cos^2\theta) \times |<f|\exp(iqr)|i>|^2 \delta(E_f - E_0 - h(v_i - v_j))$$

where $<f|$ and $|i>$ are the final and initial state wave functions, v_i and v_j are incident and scattered X-ray frequencies, θ is the scattering angle, q is the momentum transfer, and r is the distance from the nucleus. The integrand is significant only when $r <$ core hole radius. When $q\ r \ll 1$, the dipole approximation is valid and (also using $|k_i| \cong |k_j|$) the above equation becomes [22]:

$$w = \{(64\pi^5 e^4 h)/(m^2 c^2)\}(1+\cos^2\theta)\ \sin^2(\theta/2)| <i|r|f>|^2$$

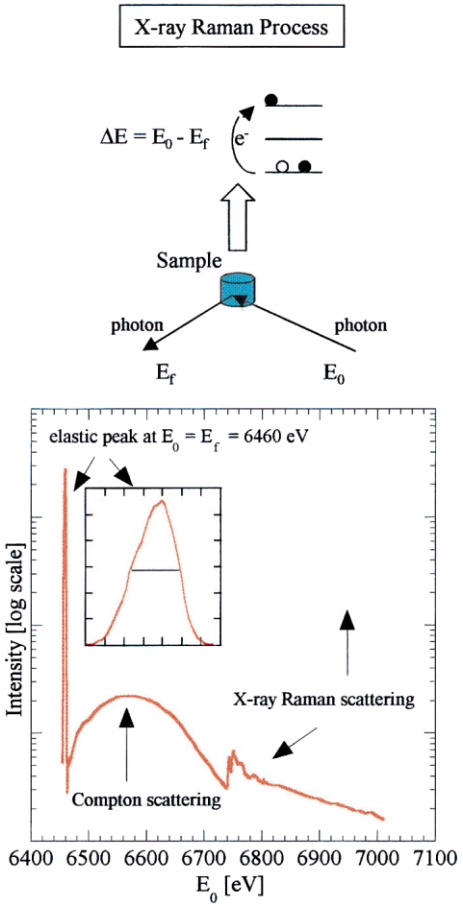

Fig. 1. (Top) An X-ray photon with incident energy E_0 is inelastically scattered with final energy E_f, providing a fraction of its energy to excite a core electron into an empty bound or continuum state. (Bottom) Rayleigh, Compton and Raman scattering profiles from graphite (note the log scale). *X*-axis shows incident photon energy at fixed analyzer setting.

where the matrix element is the same as for dipole X-ray absorption [20].

To illustrate the excellent agreement between XRS in the dipole limit and conventional XANES, Fig. 2 compares a 1 eV resolution spectrum taken on graphite in XRS mode compared to a 0.15 eV electron yield spectrum taken at the Advanced Light Sources in Berkeley [32]. The spectra also show that 1 eV resolution reveals most of the detailed spectral features.

When $qr \gg 1$, the appearance of the spectrum can change because of the contribution from non-dipole terms. This effect has been observed in the

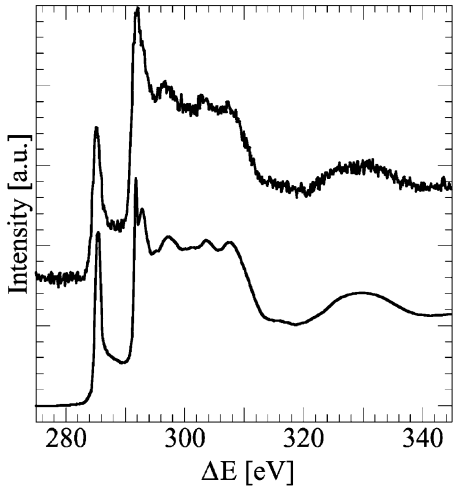

Fig. 2. Comparison of graphite K-edge XANES taken by XRS (top) with 1 eV FWHM resolution and by conventional XAS in electron yield mode (bottom) at 0.15 eV FWHM resolution. The analyzer energy was set to $E_f = 6.46$ keV, at an incident intensity of some 10^{13} photons/s.

spectrum of Li metal [25]. In the dipole limit XRS directly corresponds to conventional XAS.

4. Instrumentation

In order to be practical, an XRS experiment requires an intense monochromatic X-ray source and a large-acceptance high-resolution analyzer system. To resolve spectral features at an absorption edge, the combined monochromator/analyzer energy resolution should be ~ 1 eV or better. Flat crystals such as Si, Ge or diamond are well suited as monochromators for a collimated SR beam, but they are not efficient as analyzers for the scattered radiation. In recent years, the analyzers where usually built with cylindrically or spherically bent Ge or Si crystals.

Our instrument is based on a Johann [33] type spectrometer using spherically curved crystals. The instrument provides good energy resolution and relatively large angular acceptance. With 8.9 cm diameter Si or Ge crystals, the smallest possible spherical bending radius is slightly less than 1 m, yielding a solid angle of $\sim 6 \times 10^{-4}$ of 4π sr. We have built a multi-crystal device employing eight such analyzers on intersecting Rowland circles [34] (Fig. 3). At a Bragg angle, θ_B, of approximately 88° the spectrometer captures a solid angle of 0.5% of 4π sr. The resolution is ~ 0.3 eV at 6.46 keV using Si(4,4,0) reflections or ~ 0.5 eV at 9.7 keV using Si(6,6,0) reflections. With further optimization, a total resolution of 0.5 to 0.7 eV should be obtainable with our device; even better resolution can be obtained by systems with grooved analyzer crystals [35].

The best energy for an XRS experiment is sometimes determined by avoiding potential overlap of XRS and Compton scattering near its maximum. Other factors can include the momentum transfer q, absorption edges in the sample, and the fact that the Compton cross-section strongly increases with increasing energy. The Compton wavelength shift is $\Delta\lambda_C = \lambda' - \lambda_0 = 0.0243(1 - \cos\theta)$Å, where λ_0 and λ' are the incident and scattered wavelengths; and θ the scattering angle. This corresponds to an energy shift of $\Delta E_C =$

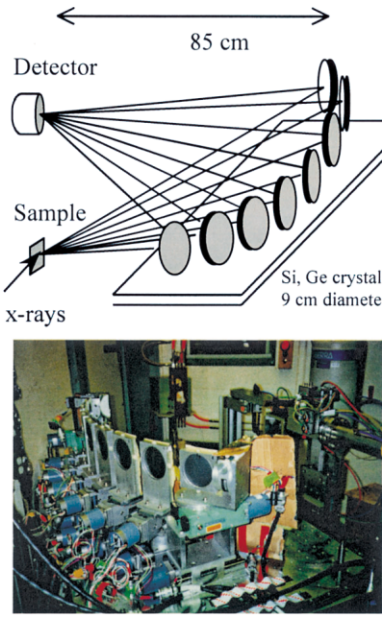

Fig. 3. High-resolution large-acceptance XRS spectrometer. Each crystal has a diameter of 8.9 cm and an 86 cm radius of curvature. The Si crystal analyzers are operated very close to backscattering in (4,4,0) or (6,6,0) reflection order, at 6.46 keV or 9.7 keV, respectively.

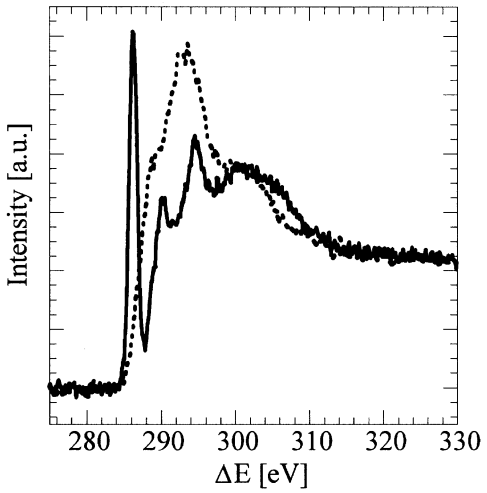

Fig. 4. XRS K-edge spectra showing extreme cases of aromatic (solid) and aliphatic hydrocarbons (dashed). The benzene (C_6H_6) spectrum was taken at a sample temperature of 10 K, the n-octacosane ($C_{28}H_{58}$) spectrum was taken at room temperature.

$E_0[\Delta\lambda_C/(\lambda_0+\Delta\lambda C)]$, which is strongly dependent on the incident energy. At large E_0 (corresponding to small λ_0) the energy shift, ΔE_C, can be very large, resulting in unwanted background in the energy range of XRS. Some typical numbers for $\theta=90^o$ are $\Delta E_C=63.6$ eV at $E_0=5.73$ keV; $\Delta E_C=112.7$ eV at $E_0=7.64$ keV; and $\Delta E_C=175.5$ eV at $E_0=9.55$ keV. The Compton spectrum shown in Fig. 1 is further broadened because of the range of scattering angles in our apparatus (see below).

Very intense X-ray sources are needed for XRS experiments, and the selected beamlines produced flux densities of up to $\sim 10^{13}$ photons/s/eV. Such high doses of radiation create substantial sample damage, and exposure times have to be kept short to avoid artifacts in the spectra. This was guaranteed by operating the beamline monochromator at APS beamline 18ID in continuous scanning mode, where a XANES scan typically took 2–3 min before the sample was automatically repositioned to a fresh spot. Depending on the data quality required and XRS intensity, 5–20 of such scans were averaged per spectrum. Unwanted background scattering was minimized by using a small detector aperture and employing a liquid nitrogen cooled low-noise Ge detector.

5. Survey of recent results

We begin the examples by comparing the C K-edge XRS for aromatic (benzene) and aliphatic (*n*-octacosane) samples (Fig. 4). The sharp low energy peak in the benzene spectrum is a $1s-\pi^*$ transition – these can only occur in systems with π bonding. The higher energy features (>290 eV) in both spectra are $1s-\sigma^*$ transitions. The energy of these resonances varies inversely with bond length. Thus, the $1s-\sigma^*$ benzene feature at 302 eV is shifted to higher energy from the same feature in n-octacosane. A detailed discussion of this correlation can be found in Stöhr's book [1]. The higher energy $1s-\sigma^*$ transitions are often referred to as 'shape resonances', because it is argued that the excited state is stabilized against immediate decay by a hump in the potential shape. An extreme example of shape resonances dominating a spectrum is the K-edge of diamond shown in Fig. 5. The raw spectrum shown here only required a total scanning time of 2 min! The much lower background contributes to the remarkable

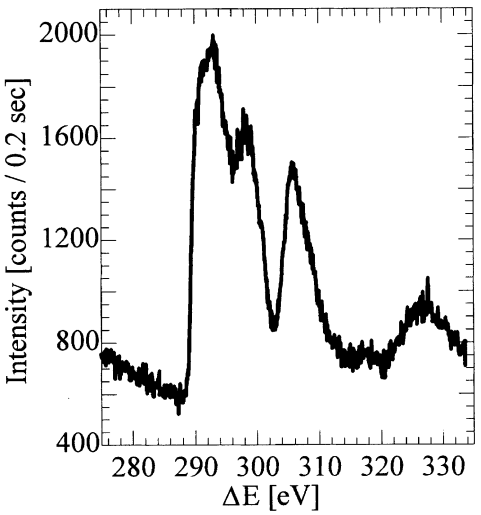

Fig. 5. Two-minute K-edge XRS raw spectrum of diamond. Incident flux $\sim 3\times 10^{13}$ photons/s, energy resolution 1 eV FWHM, $E_f=6.46$ keV.

data quality. As was seen for benzene, the characteristic diamond features are in good agreement with conventional XANES [1].

These C K-edge spectra clearly demonstrate that XRS on concentrated carbonaceous systems is not only feasible, but practical for routine bulk studies. Such work has recently been started on asphaltenes and a series of aromatic and aliphatic hydrocarbon model compounds and their mixtures [26,27]. Asphaltenes and coals represent only one class of systems that benefit from XRS analysis. There are numerous other carbonaceous systems where XRS is an essential alternative or valuable complement to conventional XANES.

Liquids are another class of samples that are troublesome (but not impossible) for soft XAS. Variation of pressure and/or temperature is especially difficult and in some cases impossible. XRS spectra of the XANES and EXAFS O K-edge for water and ice have been reported with 2 eV resolution by Borwon et al. [28]. Interestingly, these results were published before the first 'conventional' surface XANES using total ion yield and total electron yield detection on liquid water microjets [36]. This indicates the experimental difficulties conventional XAS encounters in such work (see also [37]).

Fig. 6 shows a more recent XRS spectrum of the O K-edge of water at room temperature obtained with 1 eV resolution [29]. The overall shape agrees well with the data of Bowron et al., but the better resolution reveals a pre-edge feature at 534.5 eV. This important feature is interpreted by theory as due to the donor asymmetric breaking of hydrogen bonds [37].

With a K-edge at only ~60 eV, Li is another element that is extremely difficult to study by conventional XANES (see [38] and references therein). Lithium has many important chemical and material science-related applications, e.g. in batteries and glasses, and a bulk-sensitive probe is essential. Due to the small energy transfer, the XRS signal of Li is in principle large, but there are two limiting factors. First, Compton scattering can be very strong in the range of $\Delta E = 50 - 100$ eV (see Fig. 1). Second, to obtain the full Li XRS signal, a large scattering volume is required, since each Li atom has a small scattering amplitude.

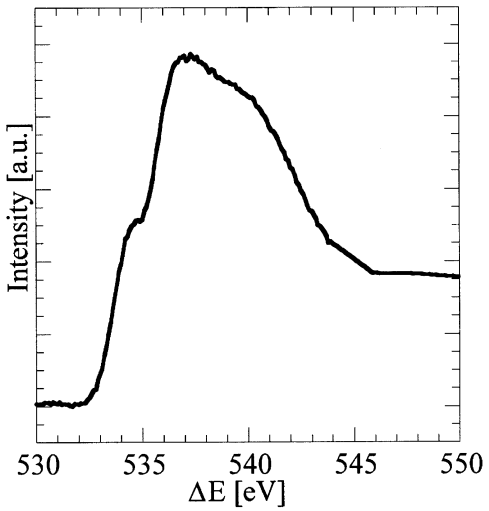

Fig. 6. O K-edge water taken in XRS mode at 9.7 keV using a Si (4,0,0) monochromator at a flux of $\sim 3 \times 10^{12}$ photons/s and Si (6,6,0) analyzers. At a resolution of 1 eV FWHM the pre-edge feature is clearly visible.

Even in concentrated Li systems this is often prevented by competition with much stronger scattering and absorption by the heavier elements in the sample. To illustrate the proportion of Compton background and XRS signal, the raw spectrum of $LiOH \cdot H_2O$ is shown in Fig. 7. Also shown is the curve fitted for Compton background subtraction. Compton scattering contributes the largest part of the signal, approximately 10 times more than XRS in the XANES region. At such a low energy transfer the XRS signal will always be on the rising side of the Compton spectrum. The decision as to what energy to use for Li XRS is, therefore, case-dependent and has to include choice of q, scattering length of the compound and Compton/XRS ratio. Fig. 8 compares XRS spectra from three Li compounds with tetrahedral O coordination. In the spectra two features, one at 60–62 eV and one at 65–68 eV are resolved. The study by Tsuji [38] on Li halides (octahedral symmetry) shows two features at similar energies shifting to higher energies with increasing ligand electronegativity. Theoretical work on understanding the observed features is currently underway.

Although our own studies have focused on energy losses of 50–600 eV, corresponding to

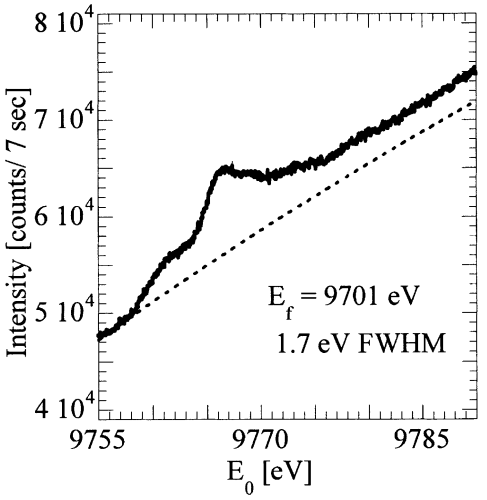

Fig. 7. Li K-edge raw spectrum of $LiOH{\cdot}H_2O$ showing large Compton scattering background. Calculated curve is used to subtract Compton background. The experiment was done with an Si 1,1,1) monochromator and Si (6,6,0) analyzers yielding a total energy resolution of 1.7 eV FWHM at an energy of E_f= 9.7 keV. The incident flux was some 10^{13} photons/s.

second row element K-edges, there is substantial interest in experiments at smaller energy losses. For example, Hayashi et al. [31] used XRS to derive the complete optical spectrum of liquid water. Fig. 9 (courtesy of Hayashi et al.) shows the optical oscillator strength of liquid water compared with that of different phases of water obtained by reflection and electron energy loss studies. Such measurements and related data at large q [39] are crucial to support simulations aimed to understand the behavior of charged particles in liquid water.

Another example of UV-like spectroscopy with hard X-rays is the study of $\pi \rightarrow \pi^*$ transitions in benzene rings [40]. At even smaller energy losses, the sample excitations correspond to localized vibrational modes or delocalized phonons [41–44]. Halcoussis et al. [45] observed O–H and O–O stretching frequencies in liquid normal and deuterated water at 0.4 ant 0.3 eV resolution respectively. Fig. 10 (reprint of Fig. 1 from [45]) shows the spectra at an energy transfer form 200–550 meV corresponding to wave numbers of 1613–4436 cm^{-1}. The signal rate was less than 1 photon/s!

One way to enhance signal rates is to exploit resonance effects. This is well known in UV-visible Raman spectroscopy, a technique often used to study dilute species. There is an analogous X-ray resonance Raman effect, which has been widely utilized in recent years. Examples include the study of electronic structure in Mott insulators [46], charge transfer excitations in NiO [47] and Nd_2CuO_4 [48] and quadrupolar transitions in Gd [49]. X-Ray resonance Raman scattering is a rapidly expanding field, but beyond the scope of this survey.

6. Summary and outlook

In this review we have focussed on XRS as a bulk-sensitive hard X-ray method for obtaining light element XANES spectra. These experiments have become possible by combining high resolution, large-acceptance X-ray optics with third generation SR sources. With incident fluxes of $\sim 10^{13}$ photons/s, XRS signal rates of up to and 10^4 photons/s at concentrated carbonaceous compounds with Compton background rates between 10^3 and 10^4 photons/s (highest for Li compounds) are observed. Sample radiation damage can be an important problem at such high incident fluxes.

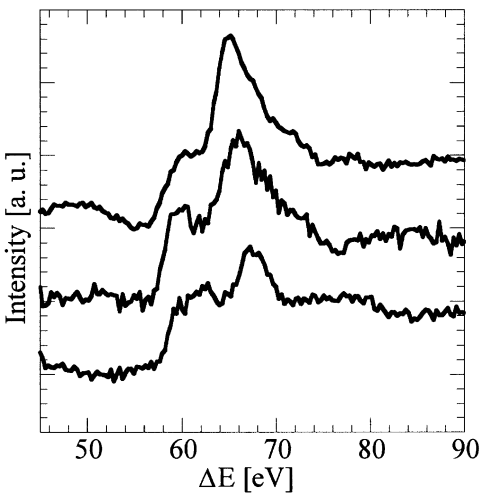

Fig. 8. Comparison of Li K-edge XRS spectra at 1.7 eV FWHM from different tetrahedrally coordinated compounds. Top to bottom: $LiOH{\cdot}H_2O$, Li_2CO_3, Li_4SiO_4.

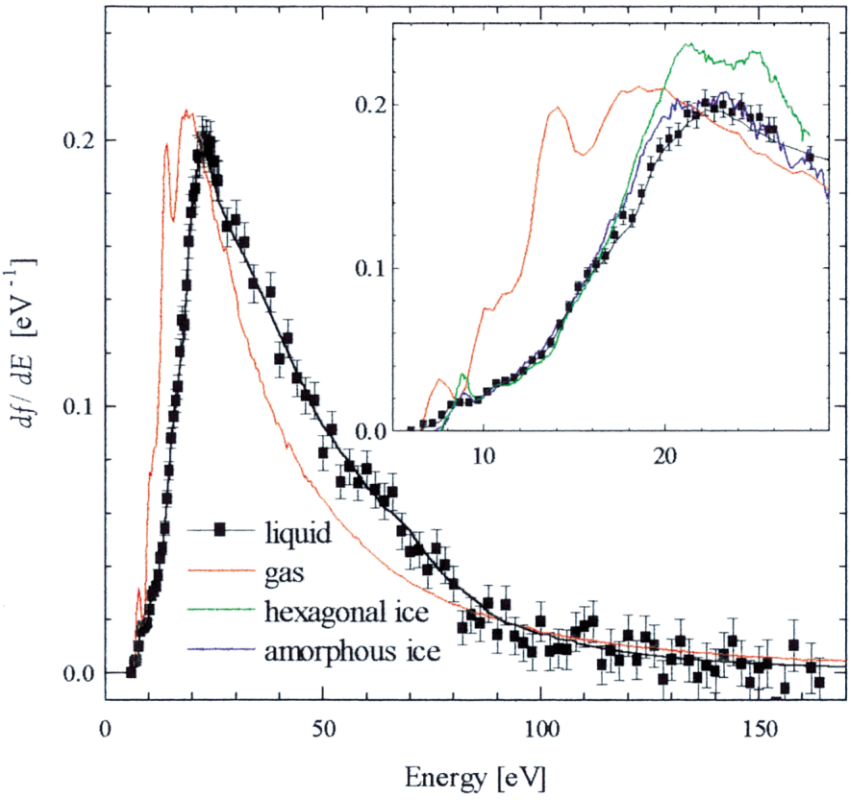

Fig. 9. Comparison of oscillator strength distribution of liquid water obtained by inelastic X-ray scattering with that of gas phase water obtained by EELS. Inset: High-resolution (0.5 eV) inelastic X-ray scattering data of liquid water compared to data of gas phase water (EELS), amorphous ice (EELS), and hexagonal ice (reflection study). Closed squares (black solid line): raw (smoothed) inelastic X-ray scattering data.

Hence, future improvements should address larger analyzer solid angle and better energy resolution as much as brighter SR sources. One proposed instrument [50] could increase efficiency by at least a factor of 10.

Anticipated fourth-generation sources will be many orders of magnitude brighter than current facilities. In some cases this might be used to facilitate vibrational XRS, while in other cases time-resolved XRS can be envisioned. Raman and Smekal would be surely amazed at what the laser has done for UV-visible inelastic scattering, and we expect the future of XRS to be equally surprising.

Acknowledgments

We thank Dr Andreas Freund for lending us the diamond crystal and the beamline staff of X-25 and 18ID for support during the experiments. This research was supported by the National Institutes of Health, grants 44891-5, GM 44380 and GM-48145, and by the Department of Energy, Office of Biological and Environmental Research. The National Synchrotron Light Source and the Advanced Photon Source are supported by the Department of Energy, Office of Basic Energy Sciences. Beamline X-25 is supported in part by the U.S. National Institutes of Health, National

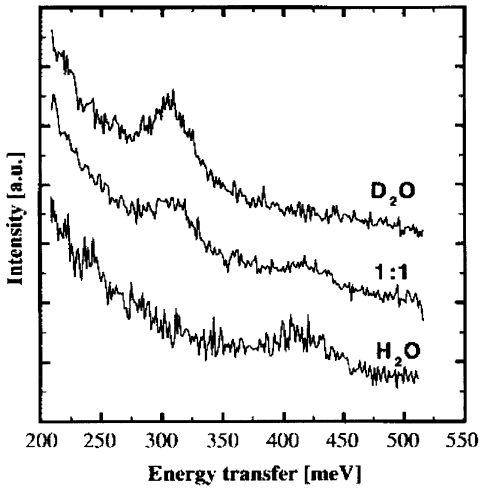

Fig. 10. Inelastic X-ray scattering spectra of the intermolecular OH and OD stretching modes of H_2O, D_2O and an H O–D_2O mixture with an equimolar H/D composition (H/D = 1:1). The spectra are vertically separated, for illustration. Intensities are given in arbitrary units. For the H_2O spectrum, a typical count rate at 400 meV was approximately 0.4–0.5 photons/s.

Center for Research Resources, and by the U.S. Department of Energy Office of Biological and Environmental Research. BioCAT is a National Institutes of Health-supported Research Center RR-08630.

References

[1] J. Stöhr, NEXAFS spectroscopy, Springer-Verlag, Berlin, New York, 1992.
[2] M. Abbate, J.B. Goedkopp, F.M.F. de Groot, et al., Surf. Interface Anal. 18 (1992) 65.
[3] J. Goulon, C. Goulon-Ginet, R. Cortes, J.M. Dubois, J. Phys. 43 (1982) 539.
[4] F.M.F. de Groot, M.-A. Arrio, P. Sainctavit, C. Cartier, C.T. Chen, Physica B 84 (1995) 208–209.
[5] B.B. Ray, Zeitschrift fuer Physik 66 (1930) 261.
[6] R.C. Majumdar, Nature 127 (1931) 92.
[7] S. Bhargava, J.B. Muckerjie, Nature 127 (1931) 273.
[8] A.J. O'Leary, Phys. Rev. 37 (1931) 873.
[9] J.M. Cork, Phys. Rev. 37 (1931) 1555.
[10] A. Sommerfeld, Phys. Rev. 50 (1936) 38.
[11] A. Smekal, Naturwissenschaften 11 (1923) 873.
[12] B. Davis, D.P. Mitchell, Phys. Rev. 32 (1928) 331.
[13] W. Ehrenberg, Zeitschrift fuer Physik 53 (1928) 234.
[14] D. Coster, I. Nitta, W.J. Thijssen, Nature 124 (1929) 230.
[15] K. Das Gupta, Nature 166 (1950) 563.
[15a] K. Das Gupta, Phys. Rev. Lett. 3 (1959) 38.
[16] K. Das Gupta, Phys. Rev. 128 (1962) 2181.
[17] K. Das Gupta, Phys. Rev. Lett. 13 (1964) 338.
[18] A. Faessler, P. Mühle, Phys. Rev. Lett. 17 (1966) 4.
[19] R.J. Weiss, Phys. Rev. 140 (1965) A1867.
[20] Y. Mizuno, Y. Ohmura, J. Phys. Soc. Jpn. 22 (1967) 445.
[21] T. Suzuki, J. Phys. Soc. Jpn. 22 (1967) 1139.
[22] K. Tohji, Y. Udagawa, Phys. Rev. B (Condensed Matter) 39 (1989) 7590.
[23] K. Tohji, Y. Udagawa, Phys. Rev. B (Condensed Matter) 36 (1987) 9410.
[24] N. Watanabe, H. Hayashi, Y. Udagawa, K. Takeshita, H. Kawata, Appl. Phys. Lett. 69 (1996) 1370.
[25] M.H. Krisch, F. Sette, C. Masciovecchio, R. Verbeni, Phys. Rev. Lett. 78 (1997) 2843.
[26] U. Bergmann, O.C. Mullins, S.P. Cramer, Anal. Chem. 72 (2000) 2609.
[27] U. Bergmann, H. Groenzin, O.C. Mullins, P. Glatzel, J. Fetzer, S.P. Cramer, submitted (2001).
[28] D.T. Bowron, M.H. Krisch, A.C. Barnes, J.L. Finney, A. Kaprolat, M. Lorenzen, Phys. Rev. B 62 (2000) R9223.
[29] U. Bergmann, P. Wernet, P. Glatzel, A. Nilsson, L.G.M. Petterson, S.P. Cramer, in preparation (2001).
[30] H. Hayashi, N. Watanabe, Y. Udagawa, C.C. Kao, J. Chem. Phys. 108 (1998) 823.
[31] H. Hayashi, N. Watanabe, Y. Udagawa, C.C. Kao, Proceedings of the National Academy of Sciences of the United States of America 97 (2000) 6264.
[32] S. Anders, J. Diaz, J.W. Ager, R.Y. Lo, D.B. Bogy, Appl. Phys. Lett. 71 (1997) 3367.
[33] H.H. Johann, Zeitschrift für Physik 69 (1931) 185.
[34] U. Bergmann, S.P. Cramer, A High-Resolution Large-Acceptance Analyzer for X-ray Fluorescence and Raman Spectroscopy, SPIE-The International Society for Optical Engineering, San Diego, California, 1998, p. 198.
[35] C. Masciovecchio, U. Bergmann, M. Krisch, G. Ruocco, F. Sette, R. Verbeni, Nuclear Instruments & Methods in Physics Research Section B-Beam Interactions With Materials and Atoms 111 (1996) 181.
[36] K.R. Wilson, B.S. Rude, T. Catalano, et al., J. Phys. Chem. B 105 (2001) 3346.
[37] S. Myneni, et al., submitted for publication (2001).
[38] J. Tsuji, K. Kojima, S. Ikeda, H. Nakamatsu, T. Mukoyama, K. Taniguchi, J. Synchrotron Radiat. 8 (2001) 554.
[39] N. Watanabe, H. Hayashi, Y. Udagawa, Bull. Chem. Soc. Jpn. 70 (1997) 719.
[40] H. Hayashi, N. Watanabe, Y. Udagawa, C.C. Kao, J. Electron Spectroscopy and Related Phenom. 114 (2001) 933.

[41] F. Sette, G. Ruocco, M. Krisch, et al., Phys. Rev. Lett. 75 (1995) 850.
[42] F. Sette, G. Ruocco, M. Krisch, C. Masciovecchio, R. Verbeni, U. Bergmann, Phys. Rev. Lett. 77 (1996) 83.
[43] G. Ruocco, F. Sette, M. Krisch, U. Bergmann, C. Masciovecchio, R. Verbeni, Phys. Rev. B-Condens. Matter 54 (1996) 14892.
[44] G. Ruocco, F. Sette, U. Bergmann, et al., Nature 379 (1996) 521.
[45] C. Halcoussis, T. Abdul-Redah, H. Neumann, G. Monaco, C.A. Chatzidimitriou-Dreismann, 2000, ESRF Newsletter, October 17.
[46] M.Z. Hasan, E.D. Isaacs, Z.X. Shen, et al., Science 288 (2000) 1811.
[47] C.C. Kao, W.A.L. Caliebe, J.B. Hastings, J.M. Gillet, Phys. Rev. B 54 (1996) 16361.
[48] J.P. Hill, C.C. Kao, W.A.L. Caliebe, et al., Phys. Rev. Lett. 80 (1998) 4967.
[49] M.H. Krisch, C.C. Kao, F. Sette, W.A. Caliebe, K. Hamalainen, J.B. Hastings, Phys. Rev. Lett. 74 (1995) 4931.
[50] U. Bergmann, R. Frahm, TDR XFEL workshop series ‘Methods and Instrumentation for the XFEL’, J. Hastings and Th. Tschentscher, eds. (2001) 52.